PCCP

PAPER

View Article Online
View Journal | View Issue

Published on 02 April 2019. Downloaded by Polska Akademia Nauk Instytut Fizyki on 5/22/2019 12:44:24 PM.

Check for updates

Cite this: *Phys. Chem. Chem. Phys.*, 2019, **21**, 8774

Computational models explain how copper binding to amyloid-β peptide oligomers enhances oxidative pathways

Giovanni La Penna *[ab] and Mai Suan Li [cd]

Received 25th January 2019,
Accepted 2nd April 2019

DOI: 10.1039/c9cp00293f

rsc.li/pccp

Amyloid-β (Aβ) peptides are intrinsically disordered peptides and their aggregation is the major hallmark of Alzheimer's disease (AD) development. The interactions between copper ions and Aβ peptides create catalysts that activate the production of reactive oxygen species in the synaptic region, a reactivity that is strongly related to AD onset. Recent experimental work [Gu *et al.*, *Sci. Rep.*, 2018, **8**(1), 16190] confirmed that the oxidative reactivity of Cu–Aβ catalyzes the formation of Tyr–Tyr crosslinks in peptide dimers. This work provides a structural basis to these observations, describing structures of Cu–Aβ dimers that enhance the propagation of the oxidative pathways activated around the Cu center. Among these, the formation of Tyr–Tyr crosslinks becomes more likely when previous crosslinks involve Cu forming bridges between different peptides. Peptides are, therefore, easily assembled into dimers and tetramers, the latter being dimers of dimers. The size of such dimers and tetramers fits with ion mobility mass spectrometry results [Sitkiewicz *et al.*, *J. Mol. Biol.*, 2014, **426**(15), 2871].

1 Introduction

Alzheimer's disease (AD) is the most representative form of dementia in humans,[1] associated with cognitive degradation caused by neuron death. Cell death is associated with the aggregation of amyloid-β (Aβ) peptides, of 39–42 amino acids, that form extracellular fibrils,[2] and with the accumulation of phosphorylated tau protein intracellularly.[3] Aβ peptides are by-products of amyloid precursor protein (APP) after its cleavage by β- and γ-secretase. Aβ monomers rapidly form oligomers, then highly-ordered insoluble proto-fibrils and eventually extended fibrils and plaques.[4,5] Soluble oligomers are toxic[2,6–8] and their role in the pathology is the subject of many studies, because of the potential role of diffusing toxic species before the aggregation process occurs.[9–13] Aβ oligomers characterized by specific toxicity are, therefore, early biomarkers of AD.

Metal ions such as zinc, copper and iron are found at high concentration in fibrils and plaques extracted from the AD-affected area of the brain.[14–19] Neurodegeneration has been linked with metal ion dishomeostasis for a long time,[20] and the interactions between metal ions and Aβ before the aggregation have been therefore investigated *in vitro*,[21] *in vivo*[22] and *in silico*.[23] Structural models of such toxic oligomers have been proposed to elucidate the mechanism by which the early events of neurodegeneration trigger irreversible neuron death, induced for instance by an increased rate of oxidation.[24–27] The role of loosely bound Cu and Fe ions in providing oxido-reductive reactivity to Aβ peptides is now well recognized *in vivo*.[28,29] Depending on the amount of reductant (or anti-oxidant) species, both intrinsic or extrinsic, the role of this oxidation can be dual:[22] on the one side, when reductant species are at low concentration, the production of reactive oxygen species (ROS) triggers the irreversible degeneration of neurons; on the other side, when the reductant concentration is high, the production of ROS triggers the degradation of the Aβ peptide itself.

Experiments *in vitro*[25,30] and computational models[24,27,31] elucidated the mechanisms of activation of dioxygen by Cu–Aβ complexes. Summarizing these observations, the mechanism begins with the formation of a small amount of reduced Cu(I)–Aβ by reductant species abundant in the central nervous system (like ascorbate). Then, the Cu(I)–O_2 pair efficiently performs an electron transfer to dioxygen, which becomes the reactive oxidant superoxide anion. The small reorganization energy of Cu with the change of oxidation state and the Cu-accessibility to solvent favour low-energy oxido-reductive cycles propagating the activation of dioxygen to superoxide and peroxide (ROS). More recently, the events that follow the activation of dioxygen have

[a] *National Research Council of Italy (CNR), Institute for Chemistry of Organometallic Compounds (ICCOM), via Madonna del Piano 10, 50019 Sesto Fiorentino, Firenze, Italy. E-mail: giovanni.lapenna@cnr.it; Fax: +39 0555225203; Tel: +39 0555225264*
[b] *Italian Institute for Nuclear Physics INFN, Section of Roma-Tor Vergata, Italy*
[c] *Institute of Physics, Polish Academy of Sciences, Al. Lotnikow 32/46, 02-668 Warsaw, Poland. E-mail: masli@ifpan.edu.pl*
[d] *Institute for Computational Science and Technology, SBI Building, Quang Trung Software City, Tan Chanh Hiep Ward, District 12, Ho Chi Minh City, Vietnam*

This journal is © the Owner Societies 2019

Published on 02 April 2019. Downloaded by Polska Akademia Nauk Instytut Fizyki on 5/22/2019 12:44:24 PM.

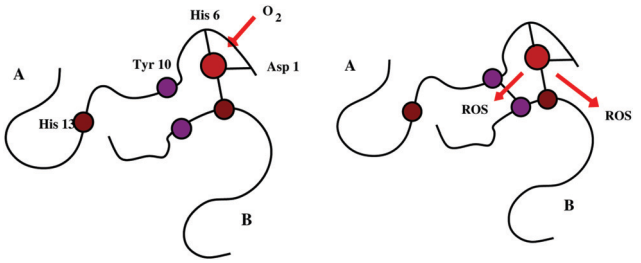

Fig. 1 A schematic picture representing the involvement of dimers in the oxidation propagation of Aβ. The activation Cu center is the large red circle; some oxidation centers are indicted: His 13 is the small red circle; Tyr 10 is the small purple circle. The flow of dioxygen towards the activation center is represented by the arrow in the left panel. The flows of ROS and of related chemical events are represented by the arrows in the right panel.

been also described.[22,32] In particular, a recent experiment[33] confirmed the observation of the formation of dityrosine (Tyr–Tyr) crosslinks in Aβ dimers because of the ROS formation in Cu–Aβ.[34,35] Since the Tyr–Tyr species can be easily measured, this observation strongly supports the opening of oxidative pathways by Cu–Aβ species.

It is well known that the production of ROS by the Cu–Aβ complex begins around one Cu binding site, because (i) of Cu accessibility to solvent and reductant species, and (ii) of the fluctuation of the reduction potential of the couple Cu(II)/Cu(I) characterizing the Cu center as a Fenton-like catalyst.[27] It is of interest to investigate, by means of molecular models, the hypothesis that, after initiation around the Cu site, ROS propagate oxidation *via* chemical reactions involving sidechains of the Cu-bound peptide and other peptides at a close distance to the activation center. In Fig. 1 a schematic drawing of this hypothesis is presented. In this work, we provide structural models of Cu–$A\beta_{42}$ dimers and tetramers where the probability of Tyr–Tyr crosslinks is enhanced. This event is particularly evident from experiments. Also, the concentration in space of most of the sidechains that can be oxidized by Cu-generated ROS (Asp 1, His, Phe, Tyr, Met) increases when dimers are crosslinked by Cu, compared to dimers with no Cu and with Cu bound to separated peptide chains.

2 Methods

2.1 Statistics

The method we used is based on the statistics of empirical models obtained by computational methods and is described in our previous work.[26,27] The sampling can be summarized as follows. Initial configurations of $A\beta_{42}$, Cu–$A\beta_{42}$, and $[Cu–A\beta_{42}]_2$ (Cu-crosslinked, see below) were selected as the most representative structures obtained with 1 μs-long molecular dynamics (MD) simulations.[26] In the first two cases, where monomers are required to build dimers, we extracted from the reported simulations of monomers the first configuration with a gyration radius (R_g) and solvent accessible surface area (SASA) corresponding to the maximum of the population for these variables obtained with the simulation. In the third case, the construction of initial configurations was different, because dimers are cross-linked by interpeptide covalent bonds involving bridging Cu atoms. Therefore, the configuration used in the first case was chosen as the initial configuration for a Monte Carlo (MC) random walk in the torsional space of the two linked monomers.[36] This type of random walk is described in detail in previous works about Cu–Aβ dimers.[37,38]

The same selection of initial configurations was adopted for dimers when the latter were used in the construction of tetramers. This time, since cross-links are confined to dimers, the selection of initial configurations was performed according to the maximally populated peak in the R_g/SASA map in all cases.

The force field was Amber 99SB[39] integrated with Cu(II).[26] The coordination of Cu was designed according to EPR experiments[40–42] displaying the Cu binding to N and O of Asp 1, Nδ(His 6) and either one of the Nδ or Nε of His 13–14. We inserted the Cu–Nε(His 13) bond. The Cu-binding to the N-terminus of Aβ is dynamic[43] and other residues are perturbed by Cu. Indeed, this dynamic behavior allows the replacement of Asp 1 by other residues with the carboxylate group, like Asp 7, Glu 3, and Glu 11, especially when the N-terminus is truncated.[44–46] In this study, the model is constrained to a fixed Cu coordination, chosen as explained above, because of the empirical model used. However, some of the important issues emerging in the literature are discussed in ''Results''.

We indicate, in the following, different monomers with different capital letters, say A, B, C, and D in the case of tetrameric assemblies. In Cu–$A\beta_{42}$ each Cu ion is bound to Asp 1(A), His 6(A) and His 13(A). In $[Cu–A\beta_{42}]_2$ one Cu ion is bound to Asp 1(A), His 6(A) and His 13(B) (Cu(A), hereafter) and the other Cu ion is bound to Asp 1(B), His 6(B) and His 13(A) (Cu(B), hereafter). This coordination is indicated as ''Cu-crosslinked'', hereafter. It must be noticed that on the time-scale of EPR and NMR experiments (ms), the intrapeptide and interpeptide Cu binding can not be distinguished, the time-scale of Cu exchange being faster than that of spectrum acquisition.[13] As examples, Fig. 2 displays two different schemes of the peptide assembly models used for Cu–Aβ dimers in this work. Tetramers are represented in a similar manner (see Table 1). We built different assemblies of A and B monomers into dimers, and of AB and CD dimers into tetramers. This was done by placing in space two particles, monomers and dimers, for building dimers and tetramers, respectively. We placed the particles with the selected structures and with random orientations with centers of mass at an approximate distance of 2 nm. The particles were inserted into orthorhombic simulation cells filled with water molecules described as in the TIP3P model[47] and a neutralizing amount of NaCl. As explained above, for the Cu-crosslinked dimer, where monomers cannot be rotated one with respect to another, a Monte Carlo procedure, performed in the dihedral space, was adopted to get a number of independent initial configurations.[38] In Fig. 3, two initial configurations used for non-crosslinked (model 2× Cu–$A\beta_{42}$) and Cu-crosslinked (model $[Cu–A\beta_{42}]_2$) are displayed in the left and right panels, respectively. We performed MD simulations in steps of 1 ns in the *NPT* statistical ensemble of 128 initial mutual orientations of the

Published on 02 April 2019. Downloaded by Polska Akademia Nauk Instytut Fizyki on 5/22/2019 12:44:24 PM.

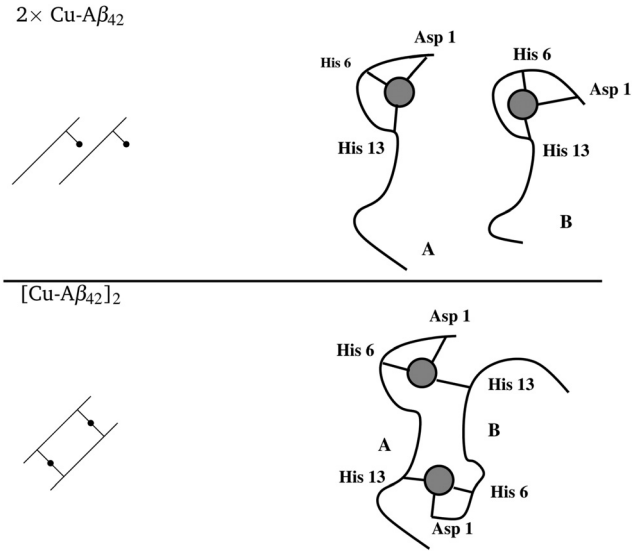

Fig. 2 Scheme of Cu-binding for the two dimeric Cu–Aβ models used in this work. In the more schematic drawings (bottom left), the black circles represent the Cu ions and the Cu-crosslinks are indicated with segments joining longer segments representing each peptide.

Table 1 Summary of the samples used to compute averages and distributions. The same schematic drawing of Fig. 2 is extended to tetramers

Model	Assembly	Walkers
	A-B	
2× $A\beta_{42}$		128
2× Cu–$A\beta_{42}$		128
$[Cu–A\beta_{42}]_2$		55
	A-B C-D	
4× $A\beta_{42}$		125
4× Cu–$A\beta_{42}$		126
2× $[Cu–A\beta_{42}]_2$		127

particles. Only in the case of Cu-crosslinked dimers the number of initial samples was 55. The pressure was 1 bar and the temperature was 300 K.

We used multiple-walker metadynamics to separate the independent trajectories, one with respect to another. The diversity among different walkers is here limited to the mutual

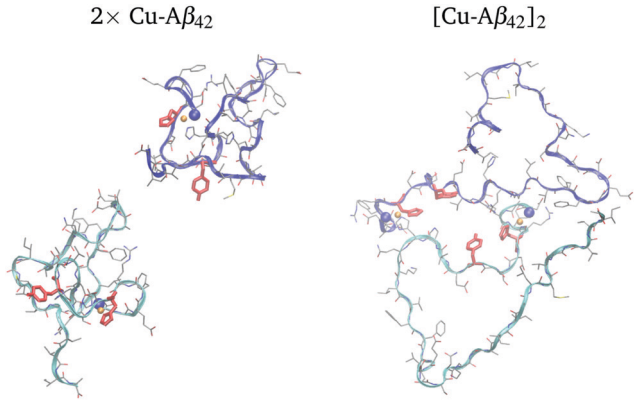

Fig. 3 Initial configurations for walker number 1 of, respectively, model 2×[Cu–Aβ42] (left panel) and $[Cu–A\beta_{42}]_2$ (right panel). Ribbons interpolate Cα atoms of the two peptides (blue and cyan, peptide A and B, respectively); blue spheres indicate the N-termini; Tyr 10 and His 6 of both A and B peptides are emphasized as red sticks; Cu ions are in orange. Atomic and bond radii are arbitrary. The drawing is performed with VMD.[48]

orientation of the peptides that form each assembly: monomers, when dimers are built; dimers, when tetramers are built. It is recommended to use a wider sampling of initial configurations. In this study we aim at investigating mainly the structural role of the presence of pre-formed Cu-crosslinks between monomers in dimeric assemblies. For this limited purpose, we performed a single multiple-walker simulation for each system, keeping the construction of the initial building blocks as similar as possible among the different simulations.

The spreading of walkers among independent trajectories was performed by adding a bias potential constructed according to the altruistic method,[49] with a collective variable chosen as the number of salt bridges within each monomer. This choice was dictated by the observation that this variable is particularly effective in changing the peptide structure,[26] thus allowing a wider sampling of different structures within the multiple walkers. After MD simulation of 20 ns in the presence of the progressively built (history-dependent) bias, 2 ns were performed with no bias. The last 1 ns was used for averaging, using one configuration every 10 ps of simulation (100 configurations per walker). Since some of the initial configurations were entangled, the latter were excluded and the number of walkers used was reduced accordingly. The metadynamics is not used here for computing the free energy, but simply to extend the sampling of different configurations as much as possible. A summary of the number of configurations used for averaging each assembly is reported in Table 1, together with schematic pictures of the peptide models. The NAMD 2.10 package[50] was used for the simulations, with most of the MD simulation parameters chosen according to standard procedures.

3 Results

3.1 Energetics: dimers and tetramers

The energy change occurring during the formation of assemblies is measured *via* the intermolecular part of dispersive

This journal is © the Owner Societies 2019

Published on 02 April 2019. Downloaded by Polska Akademia Nauk Instytut Fizyki on 5/22/2019 12:44:24 PM.

(Lennard-Jones, U_{vdw}) and Coulomb (U_q) contributions to the potential energy:

$$U_\alpha = U_\alpha(AB) - (U_\alpha(A) + U_\alpha(B)), \quad (1)$$

with α indicating the component of the potential energy, either Lennard-Jones (U_{vdw}) or Coulomb (U_q). These are the components of mechanical energy, $U_{MM} = U_{vdw} + U_q$, in the MM/PBSA (molecular mechanics Poisson–Boltzmann surface area) approximation of the free energy of protein–ligand complex formation in water solution.[51,52] The monomers are indicated as A and B in the simulations of AB dimers. Dimers AB and CD indicate the building blocks in the simulation of ABCD tetramers, and eqn (1) is modified replacing AB with ABCD, A with AB, and B with CD. As for Cu-crosslinked dimers ($[Cu–A\beta_{42}]_2$), the two crosslinking bonds (Cu(A)-B and Cu(B)-A) between, respectively, Cu(A) and peptide B and Cu(B) and peptide A, are broken and peptides B and A, respectively, are ignored when $U_\alpha(A)$ and $U_\alpha(B)$ are computed. Both energies are measured as in the simulation in the explicit solvent, but discarding the contributions of water molecules and counterions (NaCl). As for U_q, the zero-order Makov–Payne correction[53] is added, to compare systems with different net charge.

In theory, it is possible to analyze the information about water–protein and water–water interactions contained in the MD simulations. However, as expected, the thermal and volume fluctuations are too strong for such small samples to obtain a statistical mean-field convergence. In this case, the averaging over the solvent variables is performed resorting to continuum models.[51] The attempt of using MM/PBSA produced a huge dispersion of the PB (polar) and SA (non-polar) solvation free energy (data not shown here). This observation indicates the need for fine tuning of radii and other related parameters for a reliable calculation of this contribution in the case of interactions between disordered proteins, especially when the latter display very different point charge distributions because of the large structural changes occurring in the multiple-walker statistics. In the following, therefore, we analyze only the mechanical U_{MM} contribution.

To monitor the changes of MM energy with the change of structure in the simulated trajectories, we measure the extent of dimerization (dimers of monomers in the case of dimers, dimers of dimers in the case of tetramers) for each snapshot according to the R quantity,[27] which is summarized below. The quantity R is defined, for dimers of monomers, as SASA(AB)/[SASA(A) + SASA(B)], where SASA is the solvent accessible surface area of the assembly. SASA(AB) is the SASA of AB (monomers A and B in a given configuration), while SASA(A) and SASA(B) are, respectively, the SASA of the monomers A and B, in the same configuration, disregarding B and A, respectively. As for tetramers, the same equation is applied, replacing AB with ABCD, A with AB, and B with CD.

In Fig. 4, the first MM contribution (U_{vdw}) is displayed as a function of R. In all cases, the energy is divided by RT, with R the ideal gas constant and T the temperature used in the simulations (T = 300 K). The dispersive contribution decreases almost linearly with R in all cases. The slope slightly increases

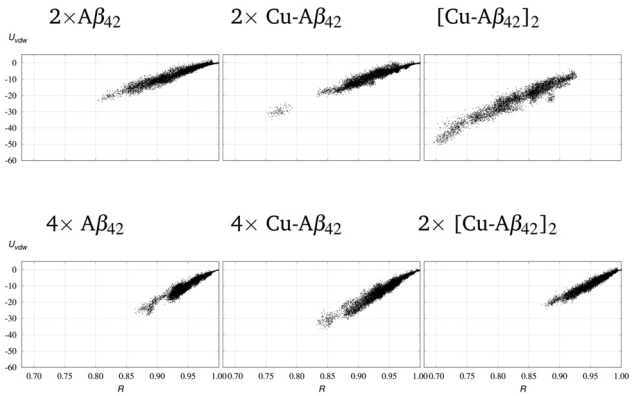

Fig. 4 The dispersive contribution to the potential energy (U_{vdw} in RT units) is plotted as a function of R, the chosen assembly parameter.

for the $[Cu–A\beta_{42}]_2$ dimer (top-right panel) with respect to the non-crosslinked dimers. As for the tetramers, the slope is about twice that of the dimers with the exception of the 2× $[Cu–A\beta_{42}]_2$ tetramer (bottom right panel). The change in the slope shows that, approximately, the total strength of dispersive interactions increases with the absolute number of sites hidden by each particle upon the formation of the assembly. This is due to the non-spherical shape of the particles involved in the assembly process. A significant extent of non-linearity occurs only for the Cu-crosslinked dimer ($[Cu–A\beta_{42}]_2$) for the low values of R. This is due to the fact that the two monomers tend to adapt their shapes to the constraints (the two Cu-crosslinks) of the preformed dimer. It must be noticed that the 2× $[Cu–A\beta_{42}]_2$ tetramer (bottom right panel) behaves very similarly to the Cu-crosslinked dimer ($[Cu–A\beta_{42}]_2$, top right panel). The similar slope of $U_{vdw}(R)$ in these two cases indicates that the energy changes in the same manner with the fraction of hidden surface and not the absolute value of the hidden surface. This means that the same fraction of hidden surface in the tetrameric case is as effective in stabilizing the tetramer as in the Cu-crosslinked dimer.

The fact that Cu-crosslinked dimers (top right panel) do not show R values larger than 0.95 indicates that the latter can be assumed as a threshold for assigning the particles to a draft assembly ($R < 0.95$) or not ($R \geq 0.95$). Therefore, in the following we use $R < 0.95$ as a criterion for assigning the assembly to a dimeric species, while $R \geq 0.95$ assigns the assembly to two separated monomers. The same criterion is used for tetramers using dimers as building particles.

Dispersive interactions are short-range, because of the distance cut-off of 1.1 nm used in simulations.[27] The contribution of long-range interactions, like the Coulomb interactions that are evaluated with no distance cut-off (because of the particle–particle particle–mesh algorithm used in the simulation), extends the picture of the forces involved in the formation of dimeric and tetrameric assemblies. In Fig. 5, $U_{MM} = U_{vdw} + U_q$ is plotted as a function of R in order to evidence the different effects of dispersive (short-range) and Coulomb (long-range) terms in the MM contribution. Beside the division by RT, the zero of the energy is chosen as the average of U_{MM} for the

Published on 02 April 2019. Downloaded by Polska Akademia Nauk Instytut Fizyki on 5/22/2019 12:44:24 PM.

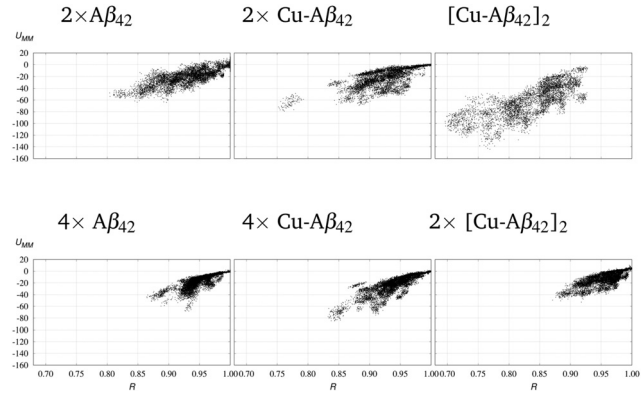

Fig. 5 The sum U_{MM} of dispersive (U_{vdw}) and Coulomb (U_q) contributions to the potential energy (in RT units) is plotted as a function of the chosen assembly parameter, R. The zero is the average of U_{MM} for points where $R = 1$.

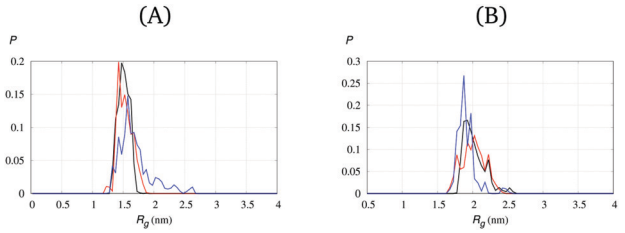

Fig. 6 Distribution (P) of the gyration radius (R_g): (A) dimers in models 2× Aβ42 (Cu-free dimers, black line), 2× Cu–Aβ42 (non Cu-crosslinked dimers, red line), and [Cu–Aβ42]2 (Cu-crosslinked dimers, blue line). (B) Tetramers in models 4× Aβ42 (Cu-free tetramers, black line), 4× Cu–Aβ42 (non Cu-crosslinked tetramers, red line), and 2× [Cu–Aβ42]2 (Cu-crosslinked tetramers, blue line). Dimers (A) and dimers of dimers (tetramers, B) are selected according to $R < 0.95$ (see the text for details). See also Table 1.

configurations with $R = 1$. The wide distribution of U_{MM} for the same values of R shows that the nature of electrostatic interactions is more diverse among the different mutual orientations of particles when the assembly is formed. There is, however, strong evidence of attractive electrostatic interactions occurring in the two dimers where Cu is present (middle and right top panels), compared to the dimers where Cu is absent (left panel). This effect is also present in tetramers (middle bottom panel compared to the left bottom panel), but the tetramers formed by two Cu-crosslinked dimers (bottom right panel) are less stabilized by electrostatic interactions than with no Cu (left panels). The latter observation is consistent with our previous observations about the change in the number of salt bridges when dimers form from monomers.[26] The intramolecular salt bridges in monomers are destabilized when dimers are formed, because the polarization induced by the Cu binding site reshuffles the charged sidechains in the monomers. Reshuffled charged groups either form new salt bridges between different monomers or increase the interactions with the polar water solvent. In the simulations reported here, the Cu-crosslinked dimers (top right panel of Fig. 5) display strong electrostatic interactions stabilizing dimers (either AB and CD). Therefore, there are no more chances for new electrostatic interactions within tetrameric assemblies formed by dimers of dimers. The compactness of the U_{MM} distribution in this case (bottom right panel) shows the nature of rigid loosely bound dimers in the case of 2× [Cu–Aβ42]2 tetramers.

As observed at the beginning of this section, the neglection of solvation and entropic effects does not allow us to draw quantitative conclusions about the free energy of protein–protein complex formation. However, we must notice that experimentally these intrinsically disordered peptides tend to form oligomeric species in short times, with low, though significant, sequence-dependent effects. This indicates that the solvation free energy, in any case, would increase the stability of oligomers compared to results of the mechanical contribution U_{MM}.

3.2 Oligomer size: dimers and tetramers

Among the most recent techniques introduced in the study of oligomers, the coupling of ion mobility with mass spectrometry (IMS-MS) allows the *in vitro*, and eventually *in vivo*, estimation of the oligomer size distribution for transient species. By using this technique, it has been possible to show differences in the oligomer size distribution between $A\beta_{40}$ and $A\beta_{42}$,[9,54] and to address the effect of the binding of $A\beta_{40}$ to metal ions such as Cu^{2+} and Zn^{2+}.[55] Despite the differences between the two peptides, a common trend is shown by experiments: monomers and oligomers become more compact when interacting with Cu, with the exception of dimers.[55,56]

According to the separation above, the distribution of the gyration radius (R_g) for the simulated dimers (Fig. 6A) shows the position of the maximally represented configurations (maxima of P) significantly shifted beyond 1.5 nm when the two Cu-crosslinks are introduced within the two monomers in dimers. We remark here that in model [Cu–Aβ42]2 the separated A and B monomers can not be formed because the A–Cu–B crosslinks are treated as fixed bonds in the empirical models used here. In our previous quantum-mechanical models we showed that this type of A–Cu–B crosslink is stable and it is not hindered by interactions between Cu-ligands.[37]

The peak position and the shape of the distribution $P(R_g)$ both indicate a significant propensity for extended configurations when the Cu-crosslinks are introduced (model [Cu–Aβ42]2), consistently with the results obtained for dimers by IMS-MS (see Fig. 3 in ref. 55).

On the other hand, the distribution of R_g for tetramers shows the compaction evidenced by IMS-MS. In Fig. 6B, the distribution $P(R_g)$ for tetramers with Cu-crosslinks displays a larger occurrence of compact configurations than for Cu-free (black line) and non Cu-crosslinked (red line) tetrameric species. The latter observation is consistent with IMS-MS data, which reveal a large peak corresponding to compact tetramers when Cu is bound to Aβ (Fig. 3, panel 3 of ref. 55).

Once the consistency of the models with the experimentally available information concerning the distribution in size of dimers and tetramers is obtained, we describe, in the following, the impact of size on the propensity to initiate and propagate oxidation events in $A\beta_{42}$, with particular emphasis on the chance of Tyr–Tyr crosslink formation.

 This journal is © the Owner Societies 2019

Published on 02 April 2019. Downloaded by Polska Akademia Nauk Instytut Fizyki on 5/22/2019 12:44:24 PM.

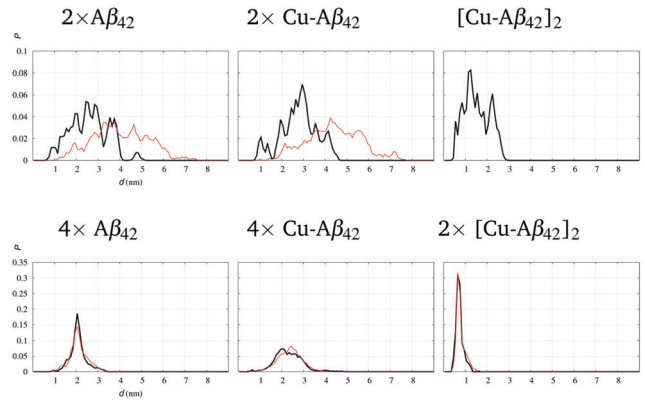

Fig. 7 Top: Distribution (P) of the distance between Cζ[Tyr(10)] in the two peptides for dimeric ($R < 0.95$, black lines) and monomeric ($R \geq 0.95$, red lines) $A\beta_{42}$ peptides (Table 1). Bottom: Same distribution in the two peptides for tetrameric ($R < 0.95$, black lines) and dimeric ($R \geq 0.95$, red lines) $A\beta_{42}$ peptides. For tetramers (bottom), only A–B and C–D pairs are displayed (Table 1).

3.3 Tyrosine–tyrosine distance: dimers

In Fig. 7, top panels, the distribution of the distance between Cζ(Tyr 10) of the two monomers is compared among the 3 analyzed dimeric assemblies, the Cu-free peptides ($2\times A\beta_{42}$, left top panel), the 1:1 Cu:Aβ system ($2\times$Cu–$A\beta_{42}$), with each Cu ion bound to a single peptide (middle top panel), and the 1:1 Cu:Aβ system, with each Cu ion binding Asp 1 and His 6 of one peptide and His 13 of the other peptide (the "Cu-crosslinked" complex, $[Cu\text{–}A\beta_{42}]_2$, right top panel). Since in model $[Cu\text{–}A\beta_{42}]_2$ there are no separated monomers, there is no red curve in the top-right panel. The comparison clearly shows that the Cu-crosslinked dimers enhance the probability of configurations with the selected distance lower than 1 nm. Structures with such a short Tyr–Tyr distance may be associated with repulsive contributions in the potential energy. Therefore, the mechanical work to produce short Tyr–Tyr distances is displayed, for dimers, in Fig. 8, where U_{vdw}(AB) and U_{MM}(AB) (see eqn (1)) are plotted as functions of the Cζ(Tyr 10 A)–Cζ(Tyr 10 B) distance analyzed in terms of probability in Fig. 7.

This figure shows that Cu-crosslinked dimers (top right) are characterized, on average, by less attractive forces compared to Cu-free peptides (top left), but there are no repulsive contributions that dominate in the total energy. Also, configurations with d below 1 nm have energy comparable (about -90 RT units) to those with no Cu. When the Coulomb term is included in U_{MM} (bottom panels), the Cu-free peptides show lower energies (with respect to the zero energy when the dimers are dissociated) compared to Cu-bound peptides. But, again, the Cu-crosslinked dimers (bottom right) display negative energy and values, at a low d distance, lower than the values for non Cu-crosslinked dimers (bottom middle). These data, together with the dimerization mechanical energy discussed in the subsection "Energetics", show that there are no repulsive forces hindering the formation of short Tyr–Tyr distances and compact entangled N-termini (see below). Most of the difference in energy between Cu-free and Cu-bound assemblies is contained in the monomers. This increase in monomeric mechanical energy is due to Cu binding, but this effect is beyond the scope of this work, while it has been discussed in ref. 26 and 56. Experiments clearly show that the binding of Cu to Aβ monomers is a spontaneous reaction,[13] even though the stability of the complex depends on the peptide sequence especially in the first residues.[45] The few computational results that include the solvation free energy change for Cu–Aβ(1–16) monomers[57] show that the Cu binding to the Aβ N-terminus is associated with a negative free energy change.

In Fig. 9 and 10, we show the structure with minimal distance d (4.5 Å) for $[Cu\text{–}A\beta_{42}]_2$, a distance not sampled in the other two models, as shown comparing the right panel with the left and middle panels in Fig. 7. The configuration of Cu(A), Tyr 10 (B) (grey), and Tyr 10 (A) (red) and the proximity of His

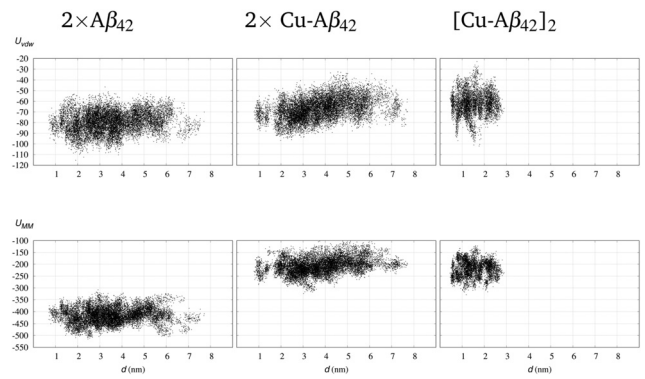

Fig. 8 Top: The dispersive contribution to the potential energy (U_{vdw}(AB), in RT units) is plotted, for dimers, as a function of the Cζ(Tyr 10 A)–Cζ(Tyr 10 B) distance (nm). Bottom: The same plot for U_{MM}(AB); in this case the zero of energy is the average of values for the points where the assembly parameter R is 1.

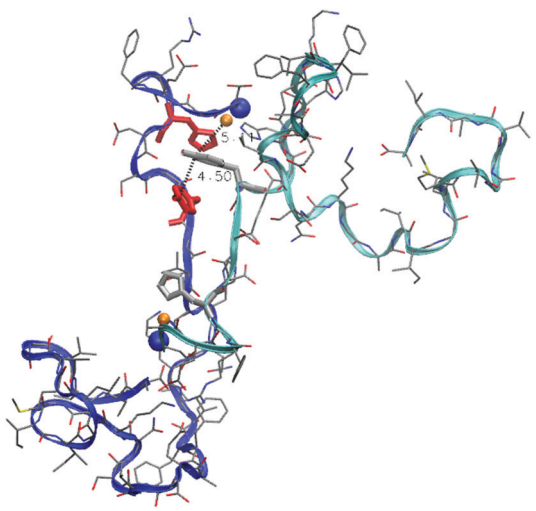

Fig. 9 Structure with the shortest distance between Cζ(Tyr 10 A) and Cζ(Tyr 10 B) (d in Fig. 7, right panel) for $[Cu\text{–}A\beta_{42}]_2$ dimers. The same drawing scheme of Fig. 3 is adopted. Tyr 10 and His 6 of peptide A are in red, while Tyr 10 and His 6 of peptide B are in grey.

Published on 02 April 2019. Downloaded by Polska Akademia Nauk Instytut Fizyki on 5/22/2019 12:44:24 PM.

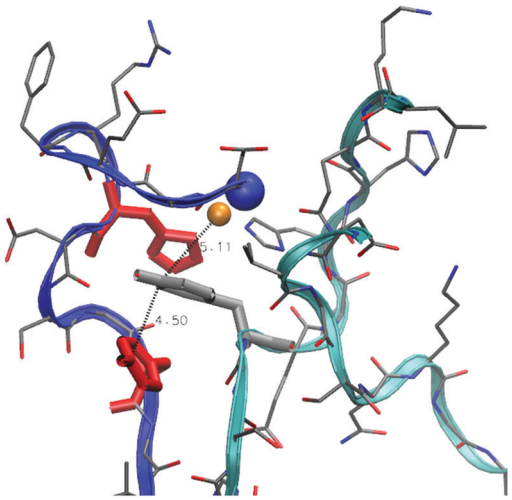

Fig. 10 Same as in Fig. 9, zoomed over Cu(A).

sidechains (His 6 of A and His 13 of B) bound to Cu(A) are molecular features assisting the electron (radical) transfer from dioxygen to Tyr 10. As already reported,[27] Cu sites in Cu–Aβ dimers are accessible to water (*e.g.* from the top of Fig. 10), and suitable to shuttle electrons from Cu(I) to dioxygen, forming superoxide ($O_2^{\bullet -}$). Therefore, the interaction between dioxygen and Cu is not hindered in dimers, while the propagation of the oxidation event to Tyr 10 is enhanced.

The minimal distance between Tyr 10 A and Tyr 10 B atoms is between two aromatic H atoms, 2.6 Å. This distance is larger than the σ parameter of the Lennard-Jones interaction between the two sites, thus the Lennard-Jones energy for that specific interaction is negative. The same holds for all the pairs of atoms belonging, respectively, to the aromatic sidechains of Tyr 10 A and Tyr 10 B: no distance is smaller than the related σ parameter. Despite the apparent crowding of aromatic sidechains displayed by this structure, no positive Lennard-Jones contributions are measured between protein atoms.

The Tyr–Tyr crosslinking is more likely in pre-formed dimers by construction, because A and B monomers are kept closer, especially in the N-terminal 1–16 region, by the covalent coordination bonds involving A–Cu–B linkages. In the initial configurations of model $[Cu–A\beta_{42}]_2$, the Cζ(Tyr 10 A)–Cζ(Tyr 10 B) distance d is almost uniformly sampled in the range 0.6 – 2.4 nm. The structure in the distribution of d (see Fig. 7, top-right panel), achieved with the multiple-walker simulation, shows a propensity to further seal pre-associated dimeric assemblies, a propensity that is less pronounced in model 2× Cu–$A\beta_{42}$ (Fig. 7, top-middle panel), even limiting the observation to the 0–2.5 nm range. As already observed in our previous Cu–Aβ models, the Cu-bound dimers are often sealed by electrostatic interactions.[26] This effect is confirmed by the analysis of the mechanical dimerization energy reported above (Fig. 5).

3.4 Tyrosine–tyrosine distance: tetramers

The same analysis has been performed for simulated tetramers. In Fig. 7, bottom panels, the distribution of the distance between Cζ(Tyr 10) is plotted for Tyr pairs belonging to the monomers involved in the initial AB and CD dimers. The other pairs display broad distributions with few samples in the 1–2 nm range and are not discussed here. The narrow peak corresponding to the Cu-crosslinked dimers assembled into tetramers (right bottom panel, both lines) clearly shows the effect on Tyr pairs of Cu-crosslinked dimers, while the broader distribution observed when Cu is bound to a single peptide chain (middle bottom panel) shows that in this case there is an opposite effect, decreasing the chance of Tyr–Tyr bonding even within a pre-associated dimer.

3.5 Other oxidation targets: dimers

The production of superoxide or hydroxyl radicals in the proximity of the Cu-binding site can produce oxidized species in several sites in the amyloid peptide, beyond Tyr 10.[22,32] As a general rule, among the oxidizable sites, Asp 1, Phe, His, Tyr, and Met sidechains are the most sensitive peptide portions. The chance to have oxidation in one of these sidechains can be measured by the chance to have in the same region of space Cu and the above sidechains. We measure this chance *via* the distribution of the gyration radius, where the latter quantity is limited to the heavy (non-H) atoms belonging to the listed sidechains. Different measures arise when counting separated monomers (indicated with A and B letters) in dimers, and the entire dimers (indicated as AB). The gyration radius extended to AB dimers indicates if the sidechains of different monomers tend to concentrate around Cu, irrespective of the involvement of sidechains in each monomer peptide sequence. The gyration radius (R_g) limited to sidechain targets of oxidation in monomer A is indicated as $R_{g,ox}$(A), while that of those sidechains of monomer B and dimer AB is indicated, respectively, as $R_{g,ox}$(B) and $R_{g,ox}$(AB).

In Fig. 11 the distribution of $R_{g,ox}$ is displayed, separately for monomers (right) and dimers (left), according to the ratio R chosen as the assembly parameter (see above). $R_{g,ox}$(A) and $R_{g,ox}$(B) are displayed, for each assembly, in black, while $R_{g,ox}$(AB) is displayed in red. Monomers (right panels) clearly show that the selected sidechains of each monomer tend to be concentrated at about $R_{g,ox} \sim 1$ nm, with the distribution for non Cu-crosslinked dimers (middle left panel) only slightly narrower than with no Cu (top left panel). Separated monomers populate configurations where the $R_{g,ox}$(AB), *i.e.* the group containing selected sidechains of both monomers, is larger than 2 nm (right panels). The Cu-crosslinked dimers (bottom left panel) display, noticeably, almost identical distributions for all sets of selected sidechains, irrespective of the monomers to which they belong. The bottom panel clearly shows that in Cu-crosslinked dimers A–B distances between oxidation targets are, on average, confined within 2 nm of those in A–A and B–B peptide pairs. On the other hand, Cu-free peptides (top) and non Cu-crosslinked Cu–Aβ (middle) assemblies show a marked difference in the degree of confinement of A–B distances compared to A–A and B–B pairs.

3.6 Other oxidation targets: tetramers

The distribution of the radius of gyration computed for sidechains suitable for oxidation ($R_{g,ox}$) is displayed in Fig. 12.

 This journal is © the Owner Societies 2019

Published on 02 April 2019. Downloaded by Polska Akademia Nauk Instytut Fizyki on 5/22/2019 12:44:24 PM.

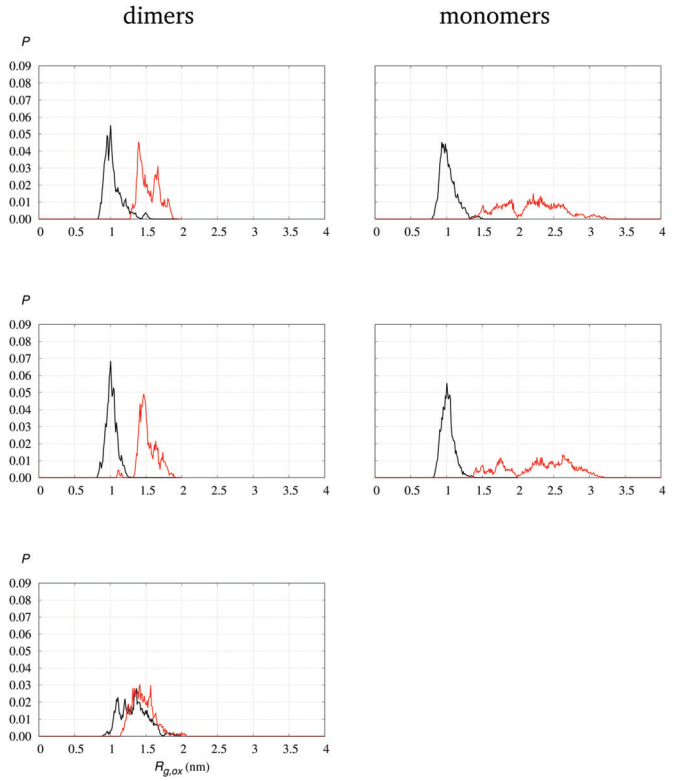

Fig. 11 Distribution (P) of the gyration radius ($R_{g,ox}$) in different $A\beta_{42}$ assemblies obtained by simulating dimers with different models: top – $2\times A\beta_{42}$; middle – $2\times$ Cu–$A\beta_{42}$; bottom – $[Cu–A\beta_{42}]_2$. Left panels: Distribution obtained for dimers ($R < 0.95$). Right panels: Distribution obtained for monomers ($R \geq 0.95$). $R_{g,ox}$ is R_g evaluated over different groups of sidechains: black lines for D1, F4, H6, Y10, H13–14, F19–20, and M35 of monomers A and B, and then averaged over monomers; red lines are for the same sidechains of dimer AB.

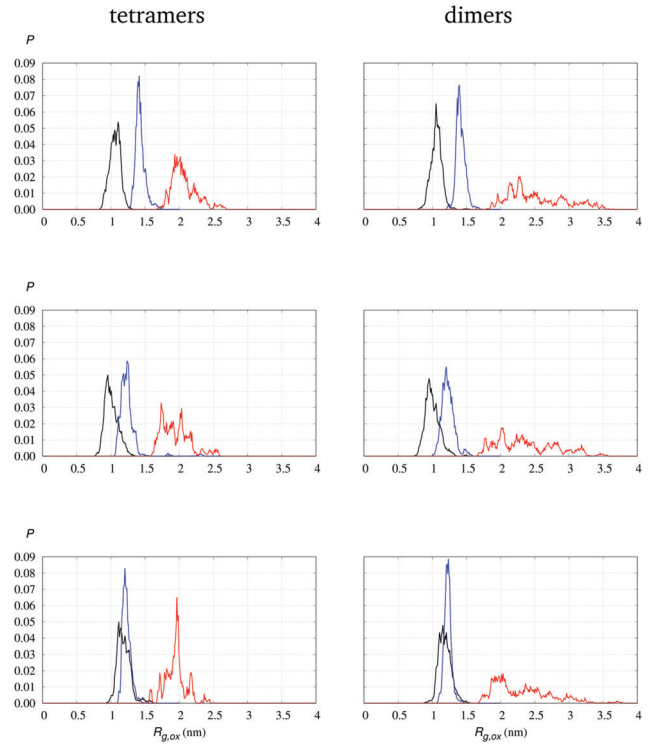

Fig. 12 Distribution (P) of the gyration radius ($R_{g,ox}$) in different $A\beta_{42}$ assemblies obtained by simulating tetramers: top – $4\times A\beta_{42}$; middle – $4\times$ Cu–$A\beta_{42}$; bottom – $2\times [Cu–A\beta_{42}]_2$. Left panels: Distribution obtained for tetramers ($R < 0.95$). Right panels: Distribution obtained for dimers ($R \geq 0.95$). $R_{g,ox}$ is R_g evaluated over different groups of sidechains: black lines for D1, F4, H6, Y10, H13–14, F19–20, and M35 of monomers A, B, C, and D, and then averaged over monomers; blue lines for the same sidechains of dimers AB and CD (averaged); red lines for the same sidechains of the ABCD tetramer.

Also in this case, the distributions computed over sidechains belonging to those dimers that are pre-associated in the simulation of tetramers are separated (blue lines). The comparison shows that the change of compaction of the selected sidechains within each monomer (black lines) is not significant (bottom panel compared to the top panel), but a significant contribution to the compaction is due to the AB and CD dimers (blue lines). The distribution for sidechains in AB and CD dimers, both in tetrameric assemblies and in separated dimers, overlaps with the distribution evaluated over single monomers. This means that two sets of sidechains (belonging to AB and CD dimers), insetad of one (each set belonging to different A–D monomers), are in the same region of space spanned by one. This effect is not dramatically enhanced in tetramers compared to dimers, thus showing that a high degree of compaction of these sidechains is already achieved in dimers.

3.7 Cu-Site perturbation towards different Cu-coordination

Despite the fixed coordination of Cu in the models, it is possible to analyze emerging perturbations of Cu sites that eventually drive the complex towards different Cu-coordination. Two important perturbations have been investigated in the recent literature. The first is the possibility for Cu to form an ATCUN-like motif when the Aβ peptide is truncated at the N-terminus.[45,46] This coordination, observed in $4–x$ and $11–x$ truncation of Cu–Aβ($1–x$) peptides, is similar to the high-affinity binding site of human seroalbumin (HSA), also in terms of oxidoreductive properties.[58] The ATCUN-like binding of Cu can be, therefore, assumed as a silenced form of Cu in the Cu–Aβ complex, compared to the full-length Cu–Aβ(1–42) peptides. The second perturbation is due to the availability of carboxylate groups (Asp and Glu) for Cu binding. In this case, computational models showed that, in certain conditions, the approach of a carboxylate group *anti* to the direction of the Cu–dioxygen interaction enhances the electron transfer from Cu(I)–Aβ to dioxygen, an event strongly activating the reduction of dioxygen.[24]

We studied, in the collected simulations, the different chances of these two kinds of perturbations of the Cu centers. As for the first perturbation (ATCUN-like motif, Xxx–Yyy–His), we measured the distance of N(Arg 5) and N(Val 12) to Cu atoms, *i.e.* Yyy = Arg 5 and Val 12. When the N(Arg 5)–Cu distance is short, the pre-organization of the Cu site towards a Phe(4)–Arg(5)–His(6) ATCUN-like motif (observed in Cu–Aβ($4–x$)) is enhanced. Similarly, the pre-organization of Glu(11)–Val(12)–His(13) is signaled by the short N(Val 12)–Cu distance.

Published on 02 April 2019. Downloaded by Polska Akademia Nauk Instytut Fizyki on 5/22/2019 12:44:24 PM.

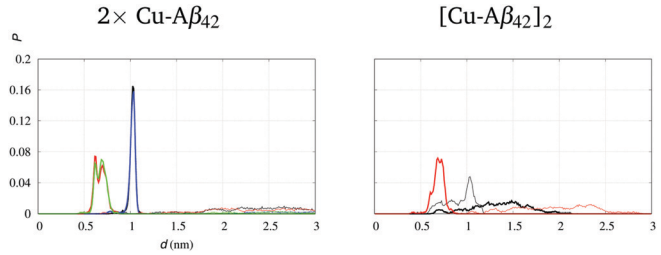

Fig. 13 Distribution (P) of the N[Val(12)]–Cu and the N[Arg(5)]–Cu distance. The drawing scheme is: thick black – N(Val 12 A)–Cu(A) in dimers ($R < 0.95$); thin black – N(Val 12 A)–Cu(B) in dimers; thick red – N(Arg 5 A)–Cu(A) in dimers; thin red – N(Arg 5 A)–Cu(B) in dimers; thick blue – N(Val 12 A)–Cu(A) in monomers ($R \geq 0.95$); thin blue – N(Val 12 A)–Cu(B) in monomers ($R \geq 0.95$); thick green – N(Arg 5 A)–Cu(A) in monomers; and thin green – N(Arg 5 A)–Cu(B) in monomers. Each distribution is the average over the permutation of A and B peptides.

In the following, we report the results for dimers, since, as shown in previous subsections, the structure of dimers is highly preserved when dimers of dimers form tetramers. The distributions of these distances are displayed in Fig. 13 for the two Cu–Aβ$_{42}$ models. The non Cu-crosslinked models (left panel) clearly show a negligible effect of dimerization (black line *versus* blue line for N(Val 12), red line *versus* green line for N(Arg 5)): both in monomers and dimers; N(Arg 5) is closer to Cu bound to the same peptide chain of the observed Arg 5 than N(Val 12). The Cu-crosslinked models (always dimers, right panel) show that N(Arg 5) (red line, right panel) is, on average, at the same distance as the non Cu-crosslinked models (red line, left panel). On the other hand, N(Val 12) is closer to Cu bound to His 13 belonging to the same chain of the observed Val 12 than in the non Cu-crosslinked model. This behavior shows that Val 12 of chain A is better wrapped around Cu(B) together with the Cu(B)-bound His 13 of the same chain A. This is an indication that in Cu-crosslinked dimers there is a larger propensity to silence the Cu ions in ATCUN-like coordination together with His 13. The His 6 sidechain does not show a different propensity in the studied models, nor in dimeric and monomeric forms.

As for the second perturbation, the distance between Cγ(Asp 1,7) and Cδ(Glu 3,11) and Cu is measured. The distribution of this distance for dimers with Cu is displayed in Fig. 14. While for the 2× Cu–Aβ$_{42}$ model there is little change in the chance of approaching Cu by carboxylate groups (blue and black lines in left panel, $d < 1$ nm), there is a significant increase in the population of distances below 0.5 nm for model [Cu–Aβ$_{42}$]$_2$ (the small peak for the black thick curve in the right panel). This behavior is a clear sign of a possible activation of electron transfer from Cu(I), once the latter is produced by reductant species in a Cu(II) not-reorganized coordination environment, towards a Cu-bound dioxygen molecule.[24,27] The simulations here reported confirm that the chance of such activation is higher when Cu-crosslinked dimers are already formed compared to Cu–Aβ dimers where the Cu-crosslinks are absent. The structure of such configurations will be investigated as activated Cu(I)–Aβ oxidation initiators, but this analysis is beyond the scope of this work, since an extended quantum-mechanical description of the Cu-site is required.

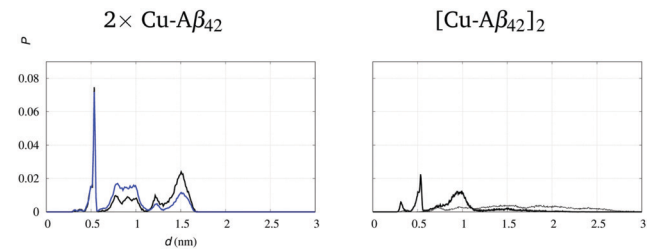

Fig. 14 Average distribution (P) of Cγ[Asp(1)]–Cu, Cδ[Glu(3)]–Cu, Cγ[Asp(7)]–Cu, and Cδ[Glu(11)]–Cu distances. Drawing scheme is: thick black – X(A)–Cu(A) in dimers ($R < 0.95$, X atoms in list above); thin black – X(A)–Cu(B) in dimers; and thick blue – X(A)–Cu(A) in monomers ($R \geq 0.95$). Each distribution is the average over the permutation of A and B peptides. A–B pairs are not displayed for 2× Cu–Aβ$_{42}$, because they are far in space.

4 Conclusions

We built models of the amyloid-β peptide 42 residues long (Aβ$_{42}$) in dimeric and tetrameric oligomers, and associated with copper coordination as indicated by *in vitro* spectroscopy. The structural models, obtained with an extended statistical method suitable to sample assemblies of intrinsically disordered proteins, show that the chance of Tyr–Tyr crosslinks and of Cu–carboxylate interactions is enhanced in dimers where each copper ion makes links between different peptides (A–Cu–B, or Cu-crosslinks), instead of being bound to a single wrapped-around peptide chain (A–Cu–A and B–Cu–B).

Therefore, our work provides a Cu-crosslinked structural model of Cu binding to Aβ$_{42}$ that is consistent with experimental observations related to Cu coordination, to oligomer size changes induced by the addition of Cu, and to Cu-induced reactivity, such as formation of Tyr–Tyr crosslinks. Taken together, these pieces of information address the diffusion of cytotoxic species prior to aggregation as a primary target for further studies of Alzheimer's disease. These models confirm that a good strategy to better understand Alzheimer's disease is to monitor early molecular events associated with oxidative stress.

Conflicts of interest

There are no conflicts to declare.

Acknowledgements

The work was supported by Narodowe Centrum Nauki in Poland (grant no. 2015/19/B/ST4/02721), by PLGrid Infrastructure (Poland), and by Department of Science and Technology at Ho Chi Minh City (Vietnam). We acknowledge PRACE for awarding us access, within the DECI 13th call, to the Eagle HPC cluster based in Poland at Poznan. The Cineca (I) HPC infrastructure is also acknowledged for the ISCRA projects awarded.

This journal is © the Owner Societies 2019

Published on 02 April 2019. Downloaded by Polska Akademia Nauk Instytut Fizyki on 5/22/2019 12:44:24 PM.

Notes and references

1 R. S. Wilson, E. Segawa, P. A. Boyle, S. E. Anagnos, L. P. Hizel and D. A. Bennett, *Psychol. Aging*, 2012, **27**, 1008–1017.
2 J. Hardy and D. J. Selkoe, *Science*, 2002, **297**, 353–356.
3 A. Alonso, T. Zaidi, M. Novak, I. Grundke-Iqbal and K. Iqbal, *Proc. Natl. Acad. Sci. U. S. A.*, 2001, **98**, 6923–6928.
4 A. W. P. Fitzpatrick, G. T. Debelouchina, M. J. Bayro, D. K. Clare, M. A. Caporini, V. S. Bajaj, C. P. Jaroniec, L. Wang, V. Ladizhansky, S. A. Müller, C. E. MacPhee, C. A. Waudby, H. R. Mott, A. De Simone, T. P. J. Knowles, H. R. Saibil, M. Vendruscolo, E. V. Orlova, R. G. Griffin and C. M. Dobson, *Proc. Natl. Acad. Sci. U. S. A.*, 2013, **110**, 5468–5473.
5 J. E. Straub and D. Thirumalai, *Annu. Rev. Phys. Chem.*, 2011, **62**, 437–463.
6 K. Chiang and E. H. Koo, *Annu. Rev. Pharmacol. Toxicol.*, 2014, **54**, 381–405.
7 S. Lesne, M. T. Koh, L. Kotilinek, R. Kayed, C. G. Glabe, A. Yang, M. Gallagher and K. H. Ashe, *Nature*, 2006, **440**, 352–357.
8 D. J. Selkoe, *Behav. Brain Res.*, 2008, **192**, 106–113.
9 S. L. Bernstein, N. F. Dupuis, N. D. Lazo, T. Wyttenbach, M. M. Condron, G. Bitan, D. B. Teplow, J.-E. Shea, B. T. Ruotolo, C. V. Robinson and M. T. Bowers, *Nat. Chem.*, 2009, **1**, 326–331.
10 S. Nag, B. Sarkar, A. Bandyopadhyay, B. Sahoo, V. K. A. Sreenivasan, M. Kombrabail, C. Muralidharan and S. Maiti, *J. Biol. Chem.*, 2011, **286**, 13827–13833.
11 E. Y. Hayden and D. B. Teplow, *Alzheimer's Res. Ther.*, 2013, **5**, 60–70.
12 M. Wolff, D. Unuchek, B. Zhang, V. Gordeliy, D. Willbold and L. Nagel-Steger, *PLoS One*, 2015, **10**, e0127865.
13 P. Faller, C. Hureau and G. La Penna, *Acc. Chem. Res.*, 2014, **47**, 2252–2259.
14 A. I. Bush, *Trends Neurosci.*, 2003, **26**, 207–214.
15 M. A. Lovell, J. D. Robertson, W. J. Teesdale, J. L. Campbell and W. R. Markesbery, *J. Neurol. Sci.*, 1998, **158**, 47–52.
16 L. M. Miller, Q. Wang, T. P. Telivala, R. J. Smith, A. Lanzirotti and J. Miklossy, *J. Struct. Biol.*, 2006, **155**, 30–37.
17 C. J. Maynard, A. I. Bush, C. L. Masters, R. Cappai and Q.-X. Lin, *Int. J. Exp. Pathol.*, 2005, **86**, 147–159.
18 K. J. Barnham and A. I. Bush, *Curr. Opin. Chem. Biol.*, 2008, **12**, 222–228.
19 K. J. Barnham and A. I. Bush, *Chem. Soc. Rev.*, 2014, **43**, 6727–6749.
20 G. Perry, L. M. Sayre, C. S. Atwood, R. J. Castellani, A. D. Cash, C. A. Rottkamp and M. A. Smith, *CNS Drugs*, 2002, **16**, 339–352.
21 P. Faller and C. Hureau, *Coord. Chem. Rev.*, 2012, **256**, 2127–2128.
22 J. Yang, X. Zhang, Y. Zhu, E. Lenczowski, Y. Tian, J. Yang, C. Zhang, M. Hardt, C. Qiao, R. E. Tanzi, A. Moore, H. Ye and C. Ran, *Chem. Sci.*, 2017, **8**, 6155–6164.
23 Y. Miller, B. Ma and R. Nussinov, *Chem. Rev.*, 2010, **110**, 4820–4838.
24 A. Mirats, J. Alí-Torres, L. Rodriguez-Santiago, M. Sodupe and G. La Penna, *Phys. Chem. Chem. Phys.*, 2015, **17**, 27270–27274.
25 K. Reybier, S. Ayala, B. Alies, J. a. V. Rodrigues, S. Bustos Rodriguez, G. La Penna, F. Collin, C. M. Gomes, C. Hureau and P. Faller, *Angew. Chem., Int. Ed.*, 2016, **55**, 1085–1089.
26 P. D. Q. Huy, Q. V. Vuong, G. La Penna, P. Faller and M. S. Li, *ACS Chem. Neurosci.*, 2016, **7**, 1348–1363.
27 G. La Penna and L. Mai Suan, *Chem. – Eur. J.*, 2018, **24**, 5259–5270.
28 A. Popa-Wagner, S. Mitran, S. Sivanesan, E. Chang and A.-M. Buga, *Oxid. Med. Cell. Longevity*, 2013, **2013**, 1–14.
29 S. Bagheri, R. Squitti, T. Haertlé, M. Siotto and A. A. Saboury, *Front. Aging Neurosci.*, 2018, **9**, 446.
30 M. Del Barrio, V. Borghesani, C. Hureau and P. Faller, *Biometals in Neurodegenerative Diseases*, Academic Press, 2017, pp. 265–281.
31 F. Arrigoni, T. Prosdocimi, L. Mollica, L. De Gioia, G. Zampella and L. Bertini, *Metallomics*, 2018, **10**, 1618–1630.
32 C. Cheignon, M. Jones, E. Atrian-Blasco, I. Kieffer, P. Faller, F. Collin and C. Hureau, *Chem. Sci.*, 2017, **8**, 5107–5118.
33 M. Gu, D. C. Bode and J. H. Viles, *Sci. Rep.*, 2018, **8**, 16190–16202.
34 C. S. Atwood, G. Perry, H. Zeng, Y. Kato, W. D. Jones, K.-Q. Ling, X. Huang, R. D. Moir, D. Wang, L. M. Sayre, M. A. Smith, S. G. Chen and A. I. Bush, *Biochemistry*, 2004, **43**, 560–568.
35 Y. K. Al-Hilaly, T. L. Williams, M. Stewart-Parker, L. Ford, E. Skaria, M. Cole, W. G. Bucher, K. L. Morris, A. A. Sada, J. R. Thorpe and L. C. Serpell, *Acta Neuropathol. Commun.*, 2013, **1**, 83.
36 G. La Penna, S. Morante, A. Perico and G. C. Rossi, *J. Chem. Phys.*, 2004, **121**, 10725–10741.
37 G. La Penna, C. Hureau, O. Andreussi and P. Faller, *J. Phys. Chem. B*, 2013, **117**, 16455–16467.
38 G. La Penna, C. Hureau and P. Faller, *Mol. Simul.*, 2015, **41**, 780–787.
39 V. Hornak, R. Abel, A. Okur, B. Strockbine, A. Roitberg and C. Simmerling, *Proteins: Struct., Funct., Bioinf.*, 2006, **65**, 712–725.
40 S. C. Drew, C. L. Masters and K. J. Barnham, *J. Am. Chem. Soc.*, 2009, **131**, 8760–8761.
41 P. Dorlet, S. Gambarelli, P. Faller and C. Hureau, *Angew. Chem., Int. Ed.*, 2009, **48**, 9273–9276.
42 D. Kim, N. H. Kim and S. H. Kim, *Angew. Chem., Int. Ed.*, 2013, **52**, 1139–1142.
43 S. C. Drew and K. J. Barnham, *Acc. Chem. Res.*, 2011, **44**, 1146–1155.
44 J. W. Karr, H. Akintoye, L. J. Kaupp and V. A. Szalai, *Biochemistry*, 2005, **44**, 5478–5487.
45 J. D. Barritt and J. H. Viles, *J. Biol. Chem.*, 2015, **290**, 27791–27802.
46 V. Borghesani, B. Alies and C. Hureau, *Eur. J. Inorg. Chem.*, 2018, 7–15.
47 W. L. Jorgensen, J. Chandrasekhar, J. D. Madura, R. W. Impey and M. J. Klein, *J. Chem. Phys.*, 1983, **79**, 926–935.
48 W. Humphrey, A. Dalke and K. Schulten, *J. Mol. Graphics*, 1996, **14**, 33–38.
49 P. Hošek, D. Toulcová, A. Bortolato and V. Spiwok, *J. Phys. Chem. B*, 2016, **120**, 2209–2215.

Published on 02 April 2019. Downloaded by Polska Akademia Nauk Instytut Fizyki on 5/22/2019 12:44:24 PM.

50 J. C. Phillips, R. Braun, W. Wang, J. Gumbart, E. Tajkhorshid, E. Villa, C. Chipot, R. D. Skeel, L. Kalé and K. Schulten, *J. Comput. Chem.*, 2005, **26**, 1781–1802.
51 P. A. Kollman, I. Massova, C. Reyes, B. Kuhn, S. H. Huo, L. Chong, M. Lee, T. Lee, Y. Duan, W. Wang, O. Donini, P. Cieplak, J. Srinivasan, D. A. Case and T. E. Cheatham, *Acc. Chem. Res.*, 2000, **33**, 889–897.
52 L. Duan, X. Liu and J. Z. Zhang, *J. Am. Chem. Soc.*, 2016, **138**, 5722–5728.
53 G. Makov and M. C. Payne, *Phys. Rev. B: Condens. Matter Mater. Phys.*, 1995, **51**, 4014.
54 M. Kłoniecki, A. Jabłonowska, J. Poznański, J. Langridge, C. Hughes, I. Campuzano, K. Giles and M. Dadlez, *J. Mol. Biol.*, 2011, **407**, 110–124.
55 E. Sitkiewicz, M. Kłoniecki, J. Poznański, W. Bal and M. Dadlez, *J. Mol. Biol.*, 2014, **426**, 2871–2885.
56 D. Q. H. Pham, M. S. Li and G. La Penna, *J. Phys. Chem. B*, 2018, **122**, 7243–7252.
57 L. Xu, X. Wang, S. Shan and X. Wang, *J. Comput. Chem.*, 2013, **34**, 2524–2536.
58 M. Sendzik, M. J. Pushie, E. Stefaniak and K. L. Haas, *Inorg. Chem.*, 2017, **56**, 15057–15065.

 This journal is © the Owner Societies 2019